Long-distance migration and venting of methane from the base of the hydrate stability zone

Richard J. Davies [1] ✉, Jinxiu Yang [2], Mark T. Ireland[1], Christian Berndt [3], Miguel Ángel Morales Maqueda[1] & Mads Huuse [4]

Marine methane hydrate is an ice-like substance that is stable in sediment around marine continental margins where water depths are greater than ~450–700 m. The release of methane due to melting of hydrates is considered to be a mechanism for past global carbon-cycle perturbations and could exacerbate ongoing anthropogenic climate change. Increases in bottom-water temperature at the landward limit of marine hydrate around continental margins, where vulnerable hydrate exists at or below the seabed, cause methane to vent into the ocean. However, this setting represents only ~3.5% of the global hydrate reservoir. The potential for methane from hydrate in deeper water to reach the atmosphere was considered negligible. Here we use three-dimensional (3D) seismic imagery to show that, on the Mauritanian margin, methane migrated at least 40 km below the base of the hydrate stability zone and vented through 23 pockmarks at the shelf break, probably during warmer Quaternary interglacials. We demonstrate that, under suitable circumstances, some of the 96.5% of methane bound in deeper water distal hydrates can reach the seafloor and vent into the ocean beyond the landward limit of marine hydrate. This reservoir should therefore be considered for estimating climate change-induced methane release during a warming world.

Gas hydrates are the most substantial store of mobile organic carbon on the Earth[1], estimated at ~1,800 GtC (ref. 2). Climatic warming causes changes in the pressure and temperature in sediment on continental margins, driving methane hydrate dissociation and the release of methane into the ocean[3]. The landward limit of the marine gas hydrate stability zone (HSZ) has been a focus of investigation, as hydrate occurs immediately below the seabed and is therefore sensitive to the warming of bottom water[3–6]. However, the volume of hydrate that is exposed during a warming event is relatively small[7]. Also, because the landward limit is located at water depths of 450–700 m, most of the gas would not reach the atmosphere[8]. Tens to hundreds of kilometres oceanward

of this exposed area, greater quantities of methane could dissociate beneath the continental slope and rise[7,9]. In this vast unexposed region, muddy and hydrate-clogged sediment layers above the methane generally prevent it from venting vertically to the ocean[10], although there are exceptional geological circumstances in which methane can migrate through the HSZ[11–13]. Permeable beds within the clinoforms that form the shelf, slope and base of the slope of continental margins could provide a route for methane to migrate up-dip[14], below the HSZ and bypassing it, to beyond its landward limit where water depths are lower at the shelf break and shelf (~100–300 m). This could be important given the amount of methane that could be released and because

[1]School of Natural and Environmental Sciences, Newcastle University, Newcastle upon Tyne, UK. [2]School of Geosciences, China University of Petroleum (East China), Qingdao, China. [3]Marine Geodynamics, GEOMAR Helmholtz-Zentrum für Ozeanforschung, Kiel, Germany. [4]Department of Earth and Environmental Sciences, University of Manchester, Manchester, UK. ✉e-mail: richard.davies@ncl.ac.uk
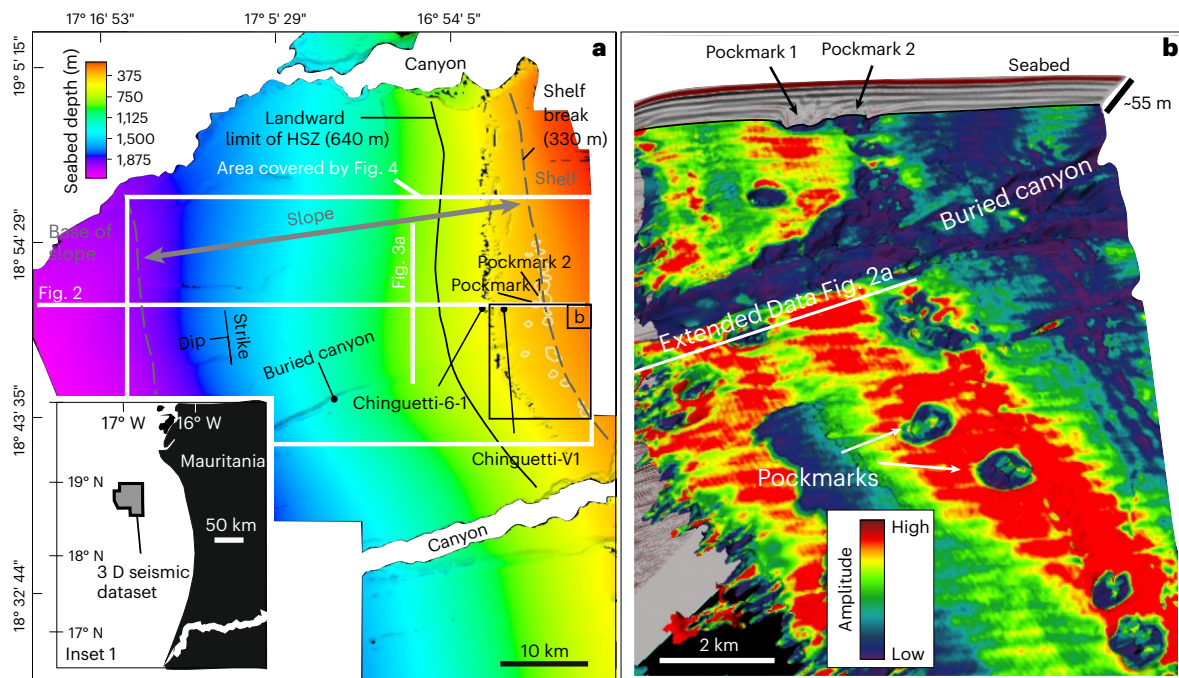
Fig. 1 | Map of the seabed offshore Mauritania from the base of the slope to the shelf break and imaging of the pockmarks, showing the locations of all other figures. a, Map of the seabed. Inset: the northwestern African margin. **b**, R.m.s. seismic amplitude map (Methods) of a reflection at the base of the field of large pockmarks in the area indicated in **a**.

thousands of vents beyond the landward limit have been observed elsewhere[15]. Also, venting in shallower water increases the chance of flux to the atmosphere[8,16].

Seismic observations

The 3D seismic data we use cover an area of 3,520 km² on the Mauritanian passive margin[17] from the shelf break to the base of the slope (330- and 2,100-m water depths, respectively)—a distance of ~64 km (Figs. 1–3). The data image hydrates and methane hosted in a set of margin-scale clinoforms, with slopes of ~2.0°. These comprise deep-water mudstones with intercalations of sands and silts[18]. Hydrocarbon boreholes show that the hydrate is within Quaternary-age sediment and that sedimentation rates have averaged at 91 m Myr⁻¹ to 116 m Myr⁻¹ (ref. 18) since the Miocene (Fig. 2). Modern and buried coral mounds[19] are located at the shelf break (Fig. 2).

The modern base of the hydrate stability zone ($BHSZ_M$) is marked by a bottom simulating reflection (BSR; Fig. 2). It dips at 2° on the slope and at 5° as it shoals to the seabed at its landward limit at ~636 m below sea level[17]. It crosscuts other reflections[17,20] and has the opposite polarity to the seabed[17,20] (Fig. 2). It is evidenced as a series of aligned high-amplitude reflection terminations (Fig. 3a, inset 1). Below the HSZ, the hydrate is not stable and there is a free-gas zone (FGZ). Deeper, relict BSRs are commonly parallel to the modern BSR and can be identified using the same criteria[21]. We selected three reflections (R1, 2 and 3; Figs. 2 and 3) that are generally parallel to each other, have a consistent vertical separation (50–150 m) and crosscut the $BHSZ_M$ and the succession immediately above and below it (Figs. 2 and 3). These are continuous for ~60 km from ~2,600 m to ~390 m below sea level. A cluster of faults intersects the succession at the base of the slope (Fig. 2). Strike and dip-parallel sections show that the succession has a synform geometry (Fig. 3a, inset 2 and Fig. 3b), the axis of which dips oceanward. The $BHSZ_M$ has the opposite geometry. It is concave downward over most of the slope. Therefore, the configuration of the strata and $BHSZ_M$ in a strike-parallel, north–south direction is that of a lens (Fig. 3a, inset 2 and Fig. 3b).

Reflections 2 and 3 include regions of high seismic amplitude that terminate abruptly (marked by yellow and green dots in Figs. 3

and 4a–c). These terminations align, to consistently define a relict BSR[21] ($BHSZ_R$) that is parallel to the $BHSZ_M$, occurring ~50 m beneath it (Fig. 3a). We modelled the position of the $BHSZ_M$ and BHSZ during the Last Glacial Maximum (LGM)[22] (Methods) over the 3D seismic survey and this predicts that they are vertically separated by 43–54 m (Fig. 3c). The mapped $BHSZ_R$ is located close to the modelled position of the BHSZ during the LGM (Extended Data Fig. 1a,b). The zone between the $BHSZ_R$ and $BHSZ_M$ is the hydrate dissociation zone (HDZ). Here, hydrate is no longer stable and methane should have been liberated. The root-mean-square (RMS) amplitude maps (Methods) for each stratal reflection (Fig. 4a–c) show that the lines of intersection for the $BHSZ_R$ and $BHSZ_M$ with reflection 1 are curved in an eastward (up-dip) and westward (down-dip) direction (Fig. 4a). The intersections of the $BHSZ_M$ and reflections 2 and 3 have the planform of a funnel (herein termed 'the funnel'), with the line of intersection (Methods)[23] between the reflections and $BHSZ_R$ remaining curved in the westward (down-dip) direction. There are also teardrop-shaped trails of higher amplitude (reflection 3) within the funnel (Fig. 4c, inset), as well as dip-parallel bands of higher seismic amplitude (marked Y in Fig. 4b,c). The intersections of reflections 1, 2 and 3 with the $BHSZ_R$ and $BHSZ_M$ can be marked by a drop or increase in seismic amplitude (Figs. 3a and 4).

Twenty-three large pockmarks occur ~10–15 km landward of the present landward limit of the HSZ (Figs. 1b and 2, inset 1). Their circular planform is very different from the carbonate mounds that form ridges in deeper water[19] (Figs. 1b and 2). They are ~50 m above reflection 1, 600–900 m wide and 20–50 m deep. Some are buried by up to 80 m of sediment (Fig. 2, inset 1), and others have an expression at the present-day seabed (Extended Data Fig. 2). They occur at a water depth of ~330 m above a series of high-amplitude black-red reflections (marked by black arrows in Fig. 2). There is a spatial coincidence between their northern limit and that of the funnel (Fig. 4b,c). The southern limit of the funnel and the pockmarks is uncertain, as the 3D seismic coverage ends. Like other examples of pockmarks[24,25], there is no evidence beneath them for vertical pathways (for example, pipes) connecting to reflections 1, 2 and 3. They are much larger than the pockmarks at the landward limit of the marine hydrate[17].
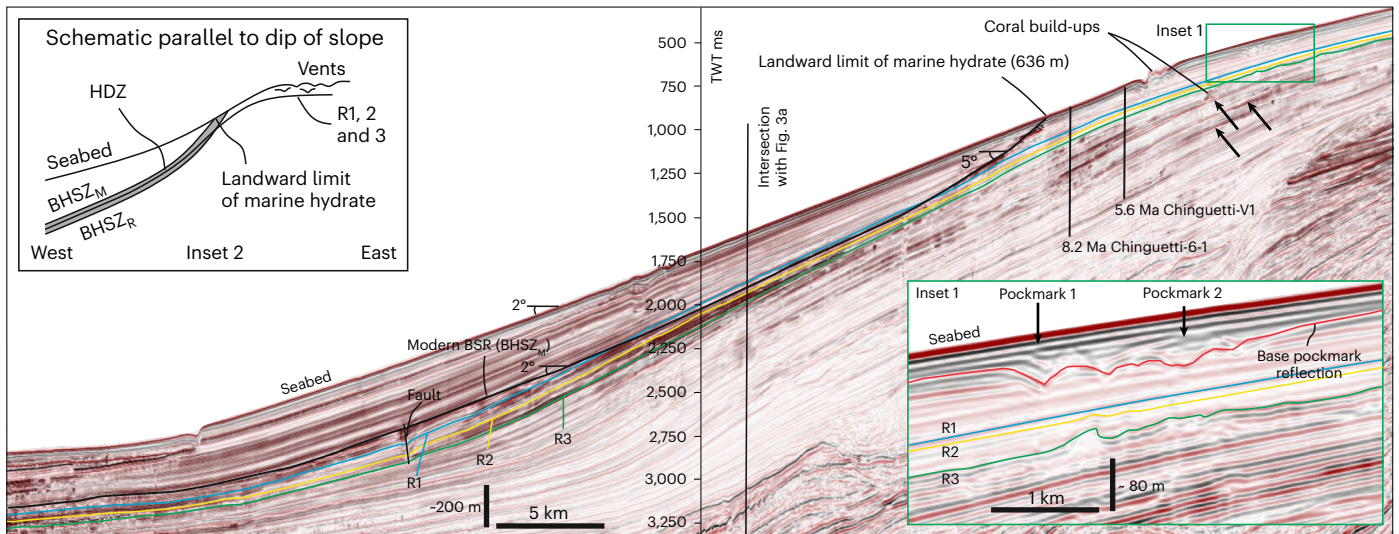
Fig. 2 | Representative seismic dip-line from the base of the slope to the shelf. The line shows the modern BSR (BHSZ$_M$), the relict BSR (BHSZ$_R$), and reflections 1, 2 and 3 (R1, 2 and 3). TWT ms, two-way travel time in milliseconds. Black arrows mark the stack of high-amplitude reflections. The two boreholes are projected locations. Inset 1: zoom-in of pockmarks 1 and 2. Inset 2: schematic of the configuration of the BHSZ$_R$, BHSZ$_M$ and reflections 1, 2 and 3.
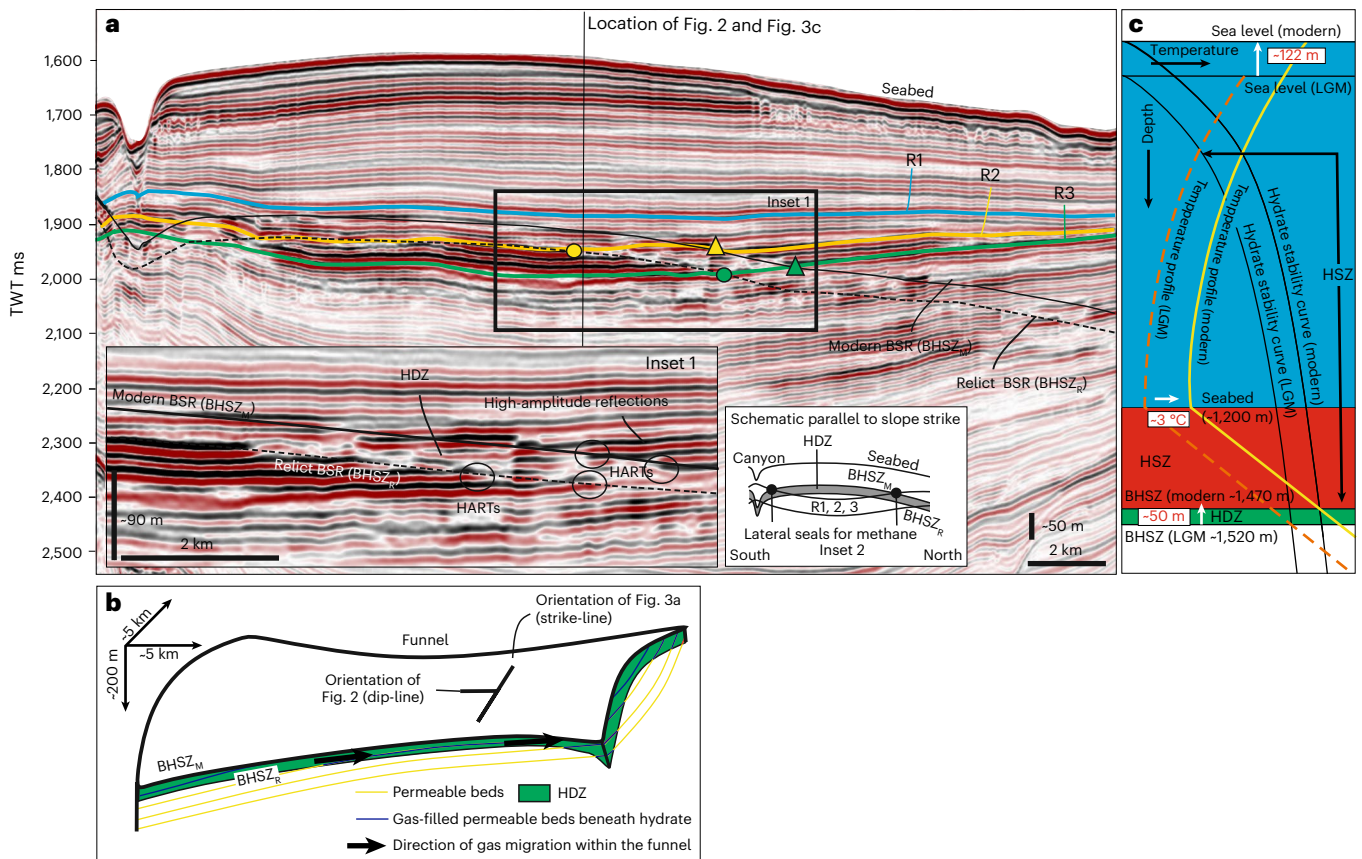

Fig. 3 | Representative seismic strike-line showing the modern and relict BSRs and the modelled magnitude of the shallowing of the BHSZ due to warming since the LGM. a, Strike-line intersecting Fig. 2. Yellow and green triangles, respectively, indicate the points of intersection of reflections 2 and 3 with the BHSZ$_M$. Yellow and green circles, respectively, indicate the points of intersection of reflections 2 and 3 with the BHSZ$_R$. Inset 1: zoom-in of the BHSZ$_R$ and BHSZ$_M$ showing the aligned high-amplitude terminations that are used to map the features. Inset 2: schematic of the configuration of the BHSZ$_R$, BHSZ$_M$

and reflections 1, 2 and 3. HARTs, high-amplitude reflection terminations. **b**, Schematic of the funnel showing the orientations of the dip and strike lines (Fig. 2 and **a**, respectively) with the stratigraphy above the BHSZ$_M$ not shown. **c**, Schematic hydrate phase diagrams for temperature–depth profiles for modern conditions (full yellow line) and those during the LGM (orange dashed line) for the location at the intersection of Fig. 2 and **a** in a mid-slope position. White boxes show the modelled magnitudes of the changes in the depth of the BHSZ, the temperature at the seabed and sea level.
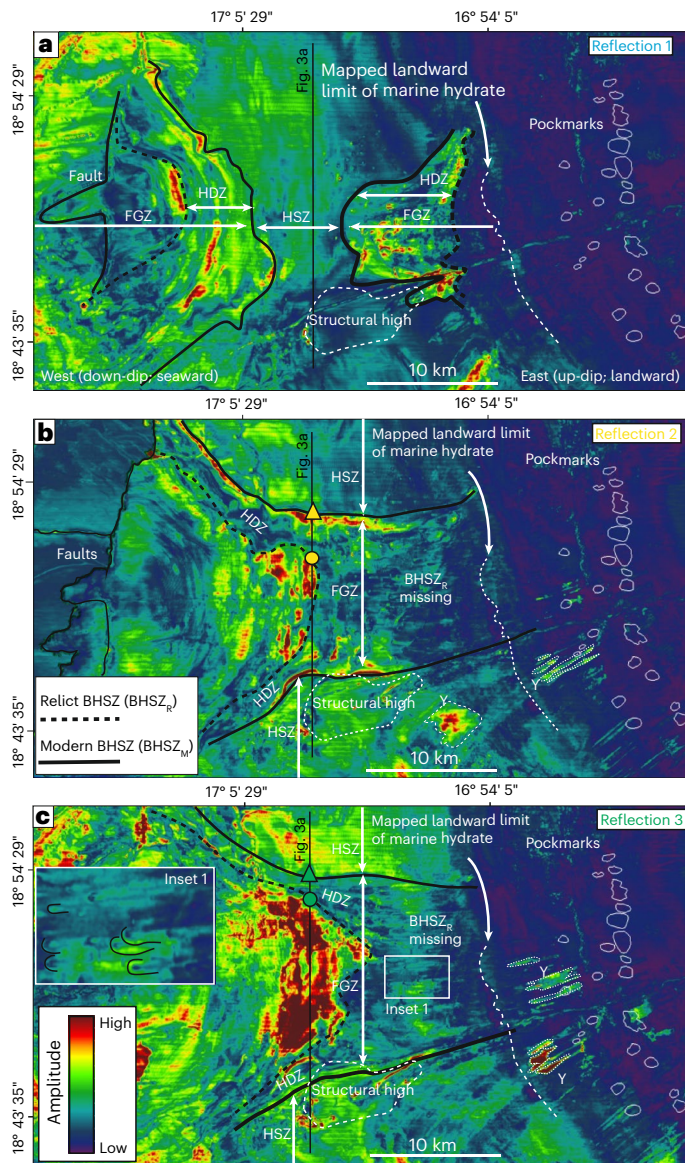
Fig. 4 | RMS amplitude maps showing the funnel and pockmarks.
a–**c**, RMS seismic amplitude maps (Methods) for reflections 1 (**a**), 2 (**b**) and 3 (**c**), respectively, showing the intersections of the BHSZ$_R$ and BHSZ$_M$, the HDZ, funnel and pockmarks. Inset 1: teardrop-shaped trails of higher seismic amplitude indicate the movement of methane below the BHSZ$_M$ (ref. 28) within the funnel, supporting the conclusion that long-distance migration of methane has occurred. Yellow and green triangles, respectively, indicate the points of intersection between reflections 2 and 3 and the BHSZ$_M$. Yellow and green circles, respectively, indicate the points of intersection between reflections 2 and 3 and the BHSZ$_R$. Y, dip-parallel bands of higher seismic amplitude.
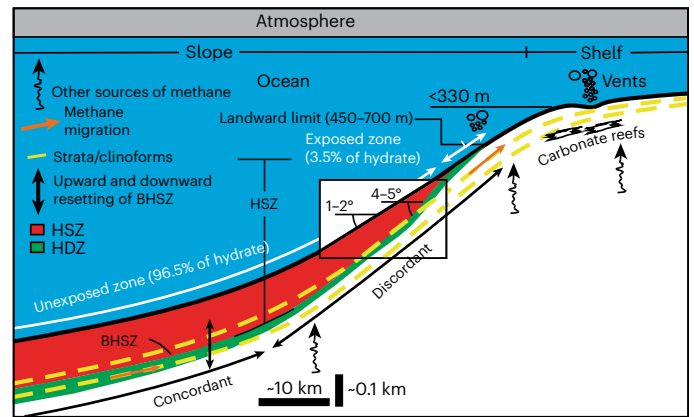

Fig. 5 | Schematic cross-section. Cross-section illustrating that the HDZ caused by a period of future climatic warming will be crosscut by continental margin clinoforms allowing methane to migrate to the shelf edge and vent beyond the landward limit of marine hydrate.

Gas migration in the HDZ

The abrupt termination, phase shift and very high amplitude of the black-red reflection terminations below the BHSZ$_M$ and BHSZ$_R$ (Figs. 2 and 3) are the result of gas beneath hydrate-clogged sediment that remained after hydrate had dissociated[21], in some cases revealing the migration pathways for the gas (Fig. 4b,c). Above the BHSZ$_M$ (Fig. 3, inset 1), high-amplitude 'hard' reflections may indicate strata with higher concentrations of hydrate[26]. The HDZ can be identified in cross-sections and map views (Figs. 2–4) and mapped over an area of over 300 km². As the three reflections are equally spaced vertically and parallel to one another, they show the intersections of the BHSZ$_R$ and BHSZ$_M$ and are

also a proxy for the three developmental stages as upward resetting of the BHSZ occurred and show how the planform of the HDZ changed (Fig. 4). The amplitude map for the shallowest reflection 1 (Fig. 4a) shows that, due to the configuration of both the BHSZ$_R$ and BHSZ$_M$ and the reflections, strata in this location were initially probably not connected within the HDZ, preventing gas from migrating up-dip through permeable beds. In contrast, during the next development stages (Fig. 4b,c) there were contiguous, permeable strata within the HDZ[27], creating a pathway for up-dip gas migration. We interpret the teardrop-shaped amplitude anomalies for reflection 3 within the funnel to be caused by the up-dip migration of methane[28], and the dip-parallel bands of high amplitudes (marked Y in Fig. 4b,c) as permeable sediments that are still gas-charged—and further evidence for migration pathways[17,20,28]. There is no evidence that the deepwater carbonates are the result of sustained seep activity. The discovery of the funnel and evidence that, within it, the HDZ is connected from its base of slope to the shelf break and to the 23 large pockmarks (Extended Data Fig. 3) are the substantive new observations.

The modelled position of the BHSZ during the LGM is very close to the BHSZ$_R$, so the BHSZ$_R$ is likely to be a feature that formed during or since the LGM. As there are no faults within the funnel, gas migration would have only been prevented by stratigraphic traps that are beyond seismic resolution[20]. South of the structural high, bands of high amplitude also occur, showing there could be other migration pathways to the south of the funnel (Extended Data Fig. 3). The BHSZ$_R$ cannot be mapped in the eastern part of the survey, probably because the strata intersecting it dip upwards away from the hydrate, so there was no trapping configuration allowing gas to pond, which would then be detected by the seismic method.

The co-location of the open eastern end of the funnel and particularly the northern boundary of the funnel and the cluster of pockmarks suggests a causal relationship. Thin deepwater sands or silts would have provided migration routes for released methane from the regions that underwent dissociation[20]. The stack of high-amplitude black-red reflections beneath the pockmarks may represent gas-charged sands, also charged by a process of up-dip gas migration. Given the sedimentation rates, burial of 80 m could have taken ~1.5 Myr (ref. 27). Some pockmarks are at the seabed and may have been active recently (Extended Data Fig. 2). Therefore, venting probably occurred episodically from the mid Quaternary and possibly to the present day. A shift of ~50 m from the BHSZ$_R$ to BHSZ$_M$ over the 300 km² of the HDZ would release ~0.023 GtCH$_4$ (with a global warming potential of 0.6 GtCO$_2$e; Methods). There are a small number of very

small pockmarks at the landward limit of the marine hydrate[17]. However, the dominant focused flow of methane into the ocean occurs after the BHSZ reset upwards, and the methane moved up-dip from a 30-km-wide zone, bypassing the HSZ and venting ~10–15 km beyond the landward limit of the hydrate. In addition to this lateral transport, it is likely that methane from deeper strata beneath the HDZ also contributed to the total volume of venting, but the absence of vertical seismic anomalies below the pockmarks suggests that this is a minor contribution.

The dip of a graded continental slope is ~2° (ref. 29). The dip of the BHSZ is at least double this at its landward limit[4] (Fig. 5). This angular discordance is common to many margins[4,15,30] (Extended Data Fig. 4). Also, in layered sedimentary rocks, horizontal permeability is higher than vertical[31]. Therefore as the BHSZ resets upwards due to climatic warming, instead of migrating along the dipping BHSZ to its landward limit[4,15], some methane should migrate up-dip along strata to beyond the landward limit of the hydrate (Fig. 5). This may also be occurring on other continental margins that share some of the characteristics of this one (Extended Data Fig. 4). This is the case, for example, on the US Atlantic Continental margin, where thousands of pockmarks have been reported on the upper slope and outer shelf, again beyond the landward limit of the HSZ[32]. The phenomenon has been documented on smaller scales elsewhere[33,34], but the process could be much more important and transport methane further, from the base of the slope to vents tens of kilometres beyond where hydrates are typically found. Even on more structurally complex margins, methane bypasses the HSZ and vents beyond the landward limit, at similar distances to those documented here[15,30]. Rather than one contiguous gas-charged bed, critical gas pressurization would have caused seal breach, allowing gas to migrate progressively up-dip (Fig. 5)[20,32]. Methane from hydrate is not considered to have had a role in Late Quaternary climatic change[35], but the occurrence of a field of large pockmarks and their connection to distal hydrate dissociation indicates that hydrate dissociation at least contributed to increased methane venting into the ocean and led to ocean acidification[36]. Previously, only ~3.5% of hydrates in the exposed zone were considered a potential climate driver[2]. However, some of the ~96.5% further down the slope can also contribute to methane venting in response to ocean warming, and this requires a reassessment of their role in climate change and potential incorporation in climate models.

Online content

Any methods, additional references, Nature Portfolio reporting summaries, source data, extended data, supplementary information, acknowledgements, peer review information; details of author contributions and competing interests; and statements of data and code availability are available at https://doi.org/10.1038/s41561-023-01333-w.

References

1. Boswell, R. & Collett, T. S. Current perspectives on gas hydrate resources. *Energy Environ. Sci.* **4**, 1206–1215 (2011).
2. Ruppel, C. D. & Kessler, J. D. The interaction of climate change and methane hydrates. *Rev. Geophys.* **55**, 126–168 (2017).
3. Skarke, A., Ruppel, C., Kodis, M., Brothers, D. & Lobecker, E. Widespread methane leakage from the sea floor on the northern US Atlantic margin. *Nat. Geosci.* **7**, 657–661 (2014).
4. Ketzer, M. et al. Gas hydrate dissociation linked to contemporary ocean warming in the southern hemisphere. *Nat. Commun.* **11**, 3788 (2020).
5. Berndt, C. et al. Temporal constraints on hydrate-controlled methane seepage off Svalbard. *Science* **343**, 284–287 (2014).
6. Ferré, B. et al. Reduced methane seepage from Arctic sediments during cold bottom-water conditions. *Nat. Geosci.* **13**, 144–148 (2020).
7. Dickens, G. R. The potential volume of oceanic methane hydrates with variable external conditions. *Org. Geochem.* **32**, 1179–1193 (2001).
8. McGinnis, D. F., Greinert, J., Artemov, Y., Beaubien, S. E. & Wüest, A. Fate of rising methane bubbles in stratified waters: how much methane reaches the atmosphere? *J. Geophys. Res.* **111**, C09007 (2006).
9. Mienert, J. et al. Ocean warming and gas hydrate stability on the mid-Norwegian margin at the Storegga Slide. *Mar. Pet. Geol.* **22**, 233–244 (2005).
10. Naudts, L. et al. Geological and morphological setting of 2778 methane seeps in the Dnepr paleo-delta, northwestern Black Sea. *Mar. Geol.* **227**, 177–199 (2006).
11. Flemings, P. B., Liu, X. & Winters, W. J. Critical pressure and multiphase flow in Blake Ridge gas hydrates. *Geology* **31**, 1057–1060 (2003).
12. Hornbach, M. J., Saffer, D. M., & Holbrook, W. S. Critically pressured free-gas reservoirs below gas-hydrate provinces. *Nature* **427**, 142–144 (2004).
13. Smith, A. J., Flemings, P. B., Liu, X. & Darnell, K. The evolution of methane vents that pierce the hydrate stability zone in the world's oceans. *J. Geophys. Res. Solid Earth* **119**, 6337–6356 (2014).
14. Dugan, B. & Flemings, P. B. Overpressure and fluid flow in the New Jersey continental slope: implications for slope failure and cold seeps. *Science* **289**, 288–291 (2000).
15. Riedel, M. et al. Controls on gas emission distribution on the continental slope of the Western Black Sea. *Front. Earth Sci.* https://doi.org/10.3389/feart.2020.601254 (2021).
16. Newman, K. R. et al. Active methane venting observed at giant pockmarks along the U.S. mid-Atlantic shelf break. *Earth Planet. Sci. Lett.* **267**, 341–352 (2008).
17. Davies, R. J., Yang, J., Li, A., Mathias, S. & Hobbs, R. An irregular feather-edge and potential outcrop of marine gas hydrate along the Mauritanian margin. *Earth Planet. Sci. Lett.* **423**, 202–209 (2015).
18. Vear, A. Deep-water plays of the Mauritanian continental margin. *Geol. Soc. Lond. Pet. Geol. Conf. Ser.* **6**, 1217–1232 (2005).
19. Colman, J. G., Gordon, D. M., Lane, A. P., Forde, M. J. & Fitzpatrick, J. J. In *Cold-Water Corals and Ecosystems* (eds Freiwald, A. & Murray Roberts, J.) 417–441 (Springer, 2005); https://doi.org/10.1007/3-540-27673-4_21
20. Davies, R. J. & Clarke, A. L. Methane recycling between hydrate and critically pressured stratigraphic traps, offshore Mauritania. *Geology* **38**, 963–966 (2010).
21. Zander, T. et al. On the origin of multiple BSRs in the Danube deep-sea fan, Black Sea. *Earth Planet. Sci. Lett.* **462**, 15–25 (2017).
22. Davies, R. J., Morales Maqueda, M. Á., Li, A. & Ganopolski, A. Millennial-scale shifts in the methane hydrate stability zone due to Quaternary climate change. *Geology* **45**, 1027–1030 (2017).
23. Davies, R. J., Thatcher, K. E., Armstrong, H., Yang, J. & Hunter, S. Tracking the relict bases of marine methane hydrates using their intersections with stratigraphic reflections. *Geology* **40**, 1011–1014 (2012).
24. Berton, F. & Vesely, F. F. Origin of buried, bottom current-related comet marks and associated submarine bedforms from a Paleogene continental margin, southeastern Brazil. *Mar. Geol.* **395**, 347–362 (2018).
25. Andresen, K. J., Huuse, M. & Clausen, O. R. Morphology and distribution of Oligocene and Miocene pockmarks in the Danish North Sea - implications for bottom current activity and fluid migration. *Basin Res.* **20**, 445–466 (2008).
26. Carcione, J. M. & Tinivella, U. Bottom-simulating reflectors: seismic velocities and AVO effects. *Geophysics* **65**, 54–67 (2000).
27. Zühlsdorff, C., Wien, K., Stuut, J.-B. W. & Henrich, R. Late Quaternary sedimentation within a submarine channel-levee system offshore Cap Timiris, Mauritania. *Mar. Geol.* **240**, 217–234 (2007).

28. Davies, R. J., Yang, J., Hobbs, R. & Li, A. Probable patterns of gas flow and hydrate accretion at the base of the hydrate stability zone. *Geology* **42**, 1055–1058 (2014).

29. Prather, B. E., O'Byrne, C., Pirmez, C. & Sylvester, Z. Sediment partitioning, continental slopes and base-of-slope systems. *Basin Res.* **29**, 394–416 (2017).

30. Riboulot, V. et al. Control of the geomorphology and gas hydrate extent on widespread gas emissions offshore Romania. *Bull. Soc. Géol. Fr.* **188**, 26 (2017).

31. Shedid, S. A. Vertical-horizontal permeability correlations using coring data. *Egypt. J. Pet.* **28**, 97–101 (2019).

32. Brothers, D. S. et al. Seabed fluid expulsion along the upper slope and outer shelf of the U.S. Atlantic continental margin. *Geophys. Res. Lett.* **41**, 96–101 (2014).

33. Rajan, A., Mienert, J. & Bünz, S. Acoustic evidence for a gas migration and release system in Arctic glaciated continental margins offshore NW-Svalbard. *Mar. Pet. Geol.* **32**, 36–49 (2012).

34. Sarkar, S. et al. Seismic evidence for shallow gas-escape features associated with a retreating gas hydrate zone offshore west Svalbard. *J. Geophys. Res. Solid Earth* **117**, B09102 (2012).

35. Sowers, T. Late Quaternary atmospheric CH_4 isotope record suggests marine clathrates are stable. *Science* **311**, 838–840 (2006).

36. Biastoch, A. et al. Rising Arctic Ocean temperatures cause gas hydrate destabilization and ocean acidification. *Geophys. Res. Lett.* https://doi.org/10.1029/2011GL047222 (2011).

Methods

Seismic data and interpretation

The 3D seismic reflection data have a bin spacing of 12.5×25 m and a vertical resolution of ~8 m. A positive increase in acoustic impedance is represented as red in the seismic sections. The data are in the time domain. We use a velocity of 1,700 ms^{-1} for sediment and 1,500 ms^{-1} for seawater to calculate sediment thickness and the depth to the seabed, respectively. An RMS amplitude map is a map of the square root of the arithmetic mean of the squares of the values of amplitude for the reflection (Figs. 1b and 4). Changes in the seismic amplitude of a reflection that crosscuts the modern and past positions of the BHSZ can be used to delineate where resetting of the BHSZ has occurred[23]. Average sedimentation rates from the two hydrocarbon exploration wells were used to estimate the age of the pockmarks.

Modelling the past position of the BHSZ

The modelled positions of BHSZ$_M$ and BHSZ$_R$ for seismic inline 12398 were calculated by using an empirical expression for the gas hydrate phase boundary, assuming pure methane and a seawater salinity of 35‰. A geothermal gradient of 42 °C km^{-1} from the seafloor to a depth of 10 km below that results in the modelled BSR matching with the observed BSR. Sea-level changes since the LGM were extracted as a time series[37], and the sea level during the LGM can be calculated by adding the changes to present-day sea level[22]. The present-day bottom-water temperature (2.39–9.08 °C) was extracted from the World Ocean Atlas around the Cap Timiris Canyon within the area 18°–22° N, 21°–17° W (ref. 38). Bottom-water temperature during the LGM was estimated by adding the past bottom-water temperature anomalies[39] to the present-day vertical temperature profile[37], and the CCSM4 climate model was used to test for a match with the observed relict BSR[22,39]. To model the modern position of the BHSZ$_M$, we used the same inputs but with the modern seabed temperature and sea level. Changes in the temperature profile of the sediment were calculated vertically using a 1D uniform and constant heat diffusivity of 10^{-6} m^2 s^{-1} and a constant geothermal gradient, with a boundary condition 10 km below the seafloor.

Estimating the weight of carbon released through the pockmarks

We measured the HDZ area within the funnel. Its thickness was modelled across the 3D survey as 43–54 m. We rounded this to 50 m. We used a porosity of 50% and a hydrate saturation of 5% (ref. 2). A volume of 1 m^3 of gas hydrate contains 164 m^3 of methane under standard conditions[40] and we multiplied the methane weight by 0.75 to calculate the carbon weight. We multiplied the methane released by 25 to obtain the CO_2-equivalent global warming potential.

Data availability

New data derived from the seismic volume and output from modelling of the position of the BHSZ during the LGM are available at https://doi.org/10.25405/data.ncl.c.6842391.

Code availability

The code and the model parameters used in this study to model the position of the BHSZ during the LGM are available at https://doi.org/10.25405/data.ncl.c.6842391.

References

37. Bintanja, R. & van de Wal, R. S. W. North American ice-sheet dynamics and the onset of 100,000-year glacial cycles. *Nature* **454**, 869–872 (2008).
38. Locarnini, M. M. et al. *World Ocean Atlas 2013 Volume 1: Temperature* (eds Levitus, S. & Mishonov, A.) NOAA Atlas NESDIS series 73 (NOAA2013).
39. Ganopolski, A. & Calov, R. The role of orbital forcing, carbon dioxide and regolith in 100-kyr glacial cycles. *Climate* **7**, 1415–1425 (2011).
40. Kvenvolden, K. A. A review of the geochemistry of methane in natural gas hydrate. *Org. Geochem.* **23**, 997–1008 (1995).
41. Kretschmer, K., Biastoch, A., Rüpke, L. & Burwicz, E. Modeling the fate of methane hydrates under global warming. *Glob. Biogeochem. Cycles* **29**, 610–625 (2015).
42. Sylvester, Z., Pirmez, C. & Cantelli, A. A model of submarine channel-levee evolution based on channel trajectories: implications for stratigraphic architecture. *Mar. Pet. Geol.* **28**, 716–727 (2011).
43. Li, A., Davies, R. J. & Mathias, S. Methane hydrate recycling offshore of Mauritania probably after the last glacial maximum. *Mar. Pet. Geol.* **84**, 323–331 (2017).
44. Wenau, S., Spiess, V. & Zabel, M. Giant seafloor depressions caused by slope failures and bottom currents on the Namibia continental margin. *Geochem. Geophys. Geosyst.* **22**, e2020GC009548 (2021).
45. Ruppel, C. D. et al. In *World Atlas of Submarine Gas Hydrates in Continental Margins* (eds Mienert, J. et al.) 287–302 (Springer, 2022); https://doi.org/10.1007/978-3-030-81186-0_24
46. Osti, G., Waghorn, K. A., Waage, M., Plaza-Faverola, A. & Ferré, B. Evolution of contourite drifts in regions of slope failures at eastern Fram Strait. *arktos* **5**, 105–120 (2019).
47. Bünz, S. & Mienert, J. Acoustic imaging of gas hydrate and free gas at the Storegga Slide. *J. Geophys. Res. Solid Earth* **109**, B04102 (2004).
48. Li, A. *Three-dimensional Seismic Analysis and Modelling of Marine Hydrate Systems Offshore of Mauritania*. PhD thesis, Durham Univ. (2017).
49. Merle, S. G. et al. Distribution of methane plumes on Cascadia margin and implications for the landward limit of methane hydrate stability. *Front. Earth Sci.* **9**, 531714 (2021).
50. Yoo, D. G. et al. Occurrence and seismic characteristics of gas hydrate in the Ulleung Basin, East Sea. *Mar. Pet. Geol.* **47**, 236–247 (2013).

Acknowledgements

Author contributions

R.J.D. interpreted the seismic data, conceived of the paper and wrote it. J.Y. edited the text and figures and calculated the methane weight. M.A.M.M. modelled the past positions of the BHSZ. M.T.I. supported the seismic interpretation and developing the concepts. C.B. and M.H. scoped and edited the paper.

## Competing interests

The authors declare no competing interests.

Additional information

Extended data is available for this paper at https://doi.org/10.1038/s41561-023-01333-w.

Correspondence and requests for materials should be addressed to Richard J. Davies.

Peer review information *Nature Geoscience* thanks Carolyn Ruppel, W. Holbrook, Kehua You and Jess Hillman for their contribution to the peer review of this work. Primary Handling Editors: James Super and Alison Hunt, in collaboration with the *Nature Geoscience* team.

Reprints and permissions information is available at www.nature.com/reprints.
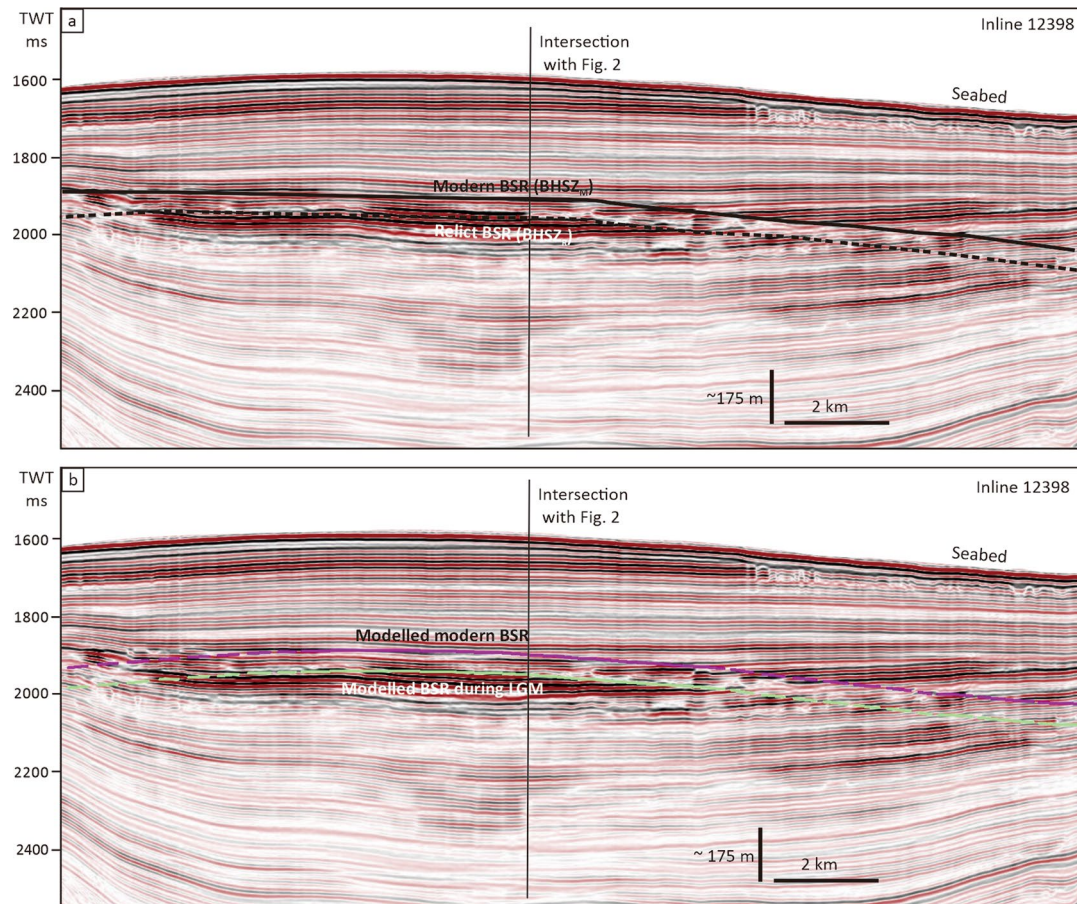
Extended Data Fig. 1 | Interpreted and modelled positions of the BHSZ for inline 12398. a) Seismic line from Fig. 3 with the interpreted modern and relict BSRs (part a) and modelled positions of the modern BSR and the BSR during the LGM (Last Glacial Maximum) (part b).
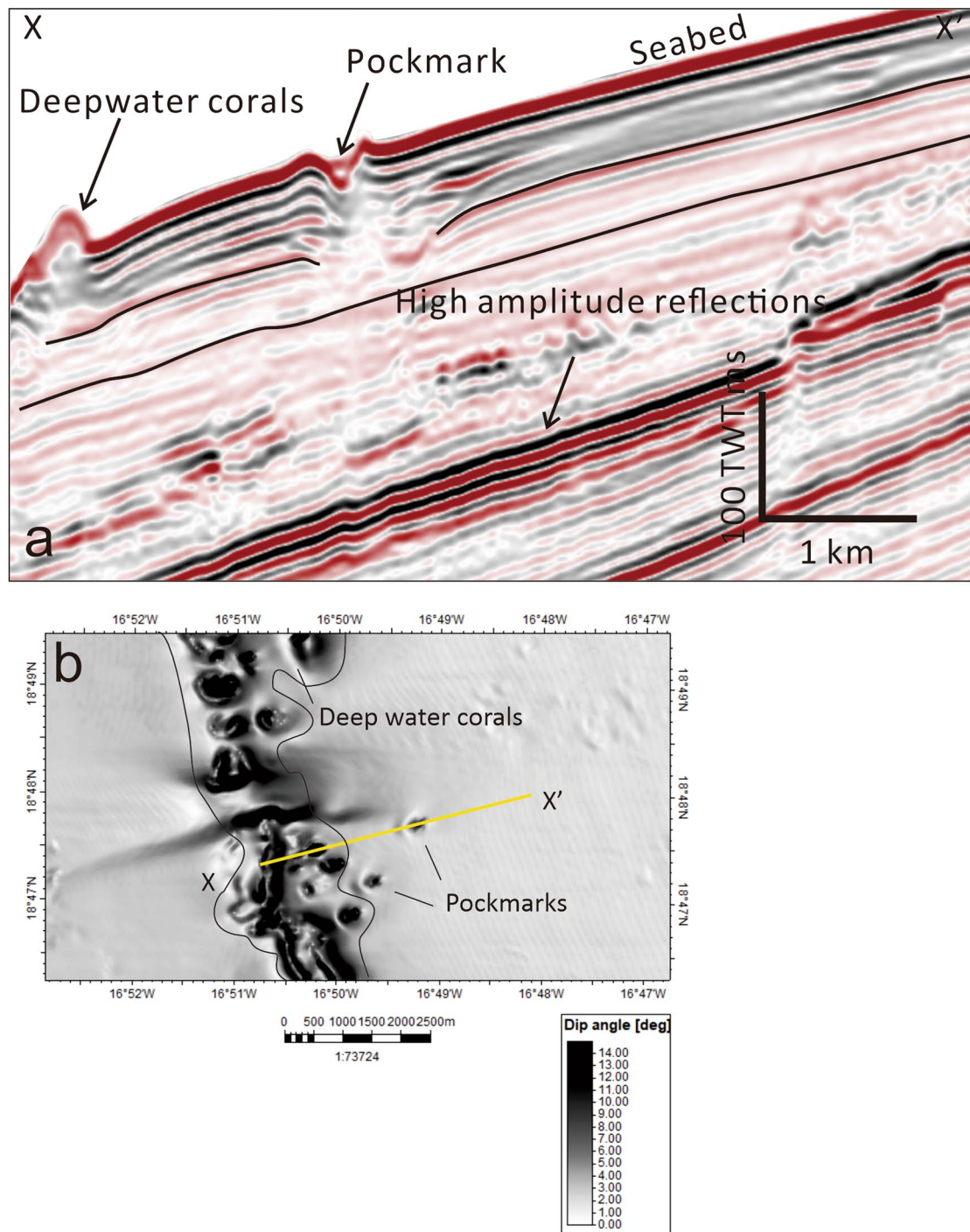
Extended Data Fig. 2 | Pockmark at the seabed. a) Seabed map showing the location of one of the 23 large pockmarks. b) Representative seismic line across the pockmark (TWT ms – two-way travel time in milliseconds).
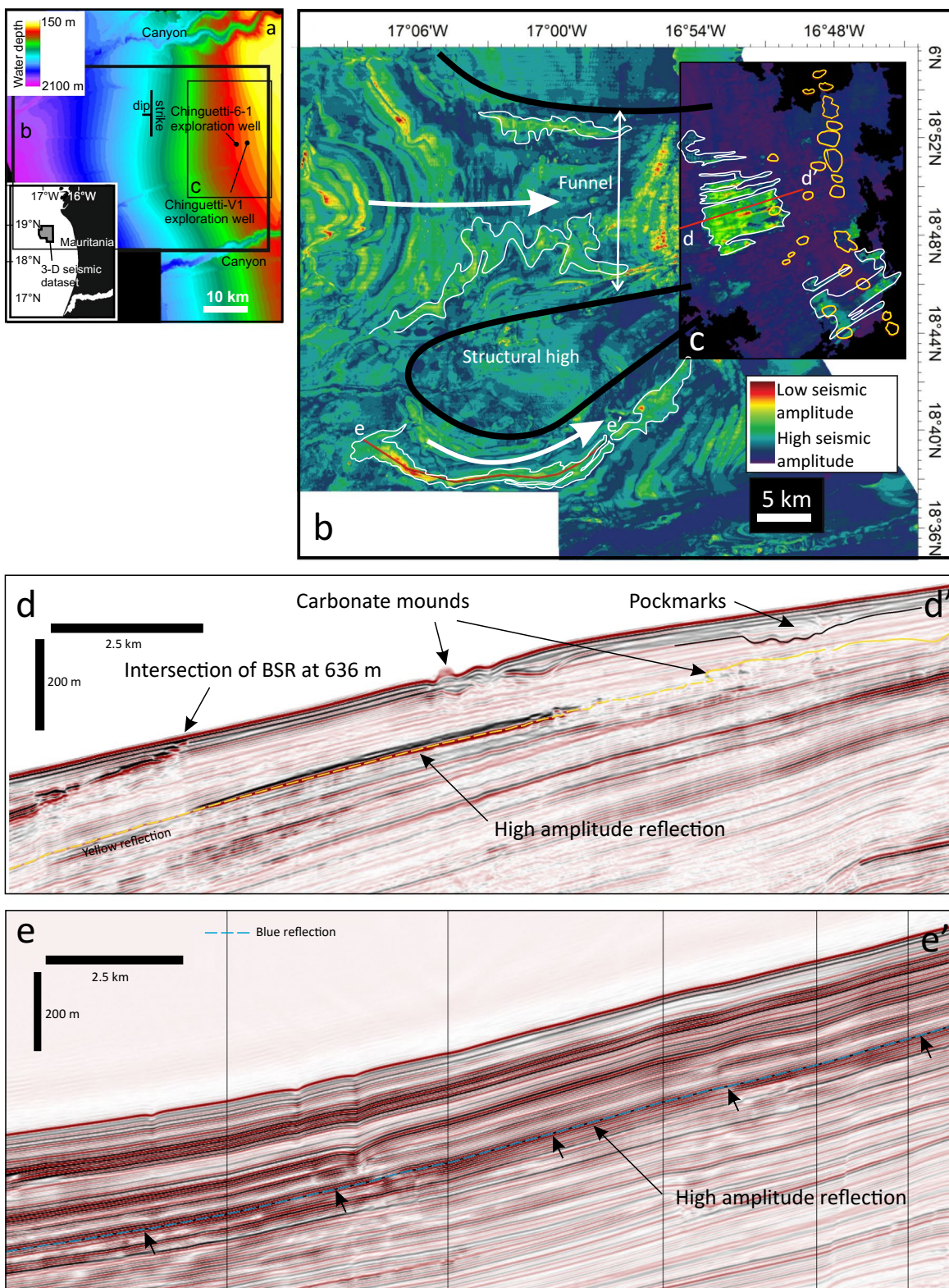
Extended Data Fig. 3 | Additional evidence for long-distance gas migration.
a) Map of the seabed from the base of slope to shelf break offshore of Mauritania.
b) RMS amplitude map (See Methods) of the modern BSR showing bands of high seismic amplitude (1, 2 and 3) indicative of gas migration beneath the hydrate
c) RMS amplitude map of an additional mapped reflection (dashed yellow reflection, R2 in d), showing areas of high seismic amplitude beyond the landward limit of hydrate. d) Seismic line d-d' showing high amplitude yellow reflection (R2) down-dip of the pockmarks. e) Seismic line e-e' showing a continuous high seismic amplitude reflection (blue dashed line) extending for ~18 km.
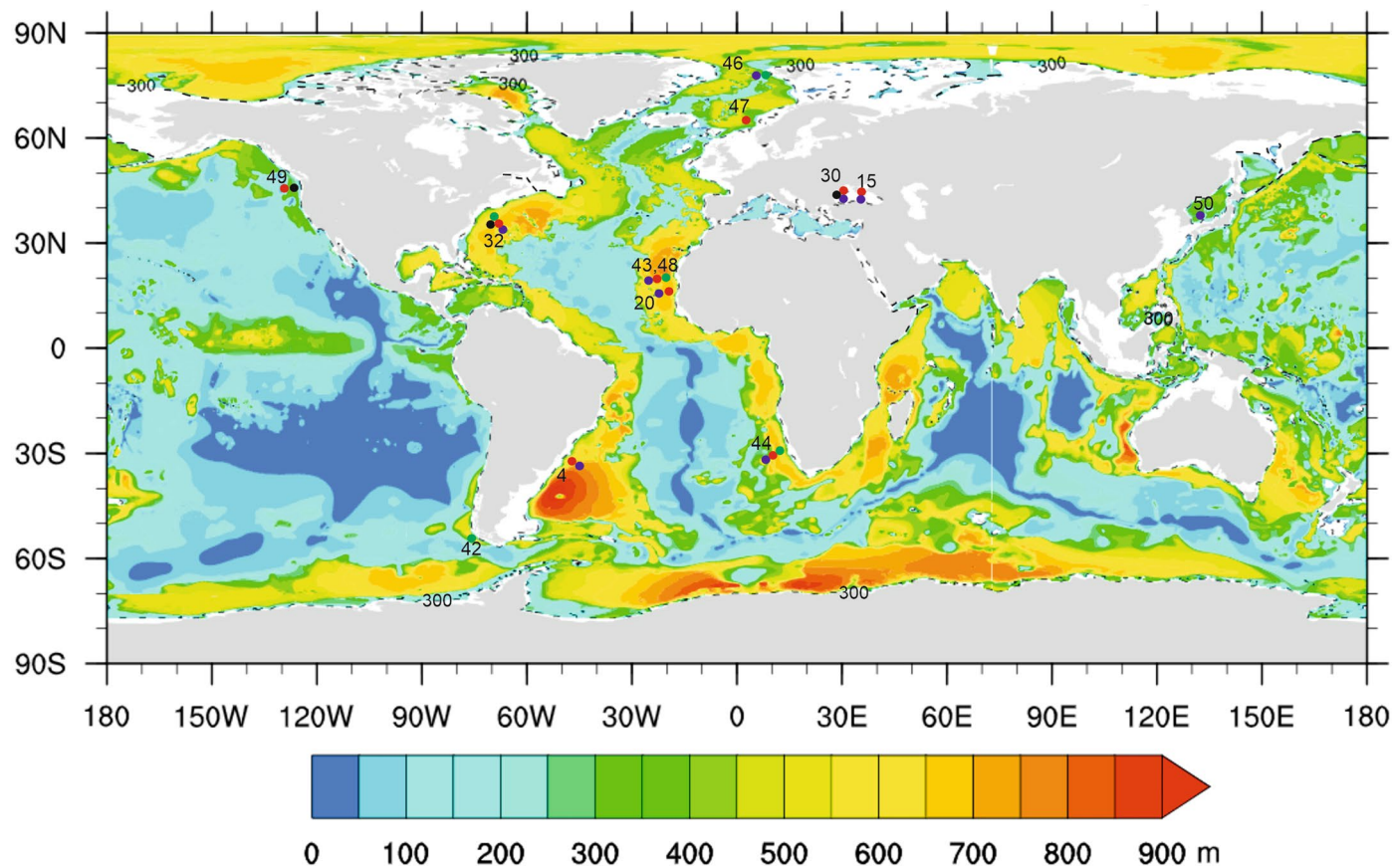
Extended Data Fig. 4 | Continental margins with similar characteristics to the Mauritanian margin and gas hydrate. Calculated thickness of the theoretical gas hydrate stability zone[41] around the globe with examples of hydrate provinces[42] hosted on continental margins with comparable characteristics. Green dots – seismic evidence for the existence of simple graded margins[32,43–46]; red dots – seismic evidence for the landward limit of marine hydrate where the dip of the BHSZ > the dip of strata[4,15,20,30,32,43,45,47–49]; blue dots – BHSZ is approximately concordant with strata on the continental slope[4,20,30,32,43–46,48,50]; black dots – pockmarks significantly (up to 10s of km) beyond the landward limit of marine hydrate[30,32,49].